Electronic Supplementary Material (ESI) for Environmental Science: Processes & Impacts.

Supplementary Information to

Interactions of ferrous iron with clay mineral surfaces during sorption and subsequent oxidation

Natacha Van Groeningen[a], Laurel K. ThomasArrigo[a], James M. Byrne[b], Andreas Kappler[b], Iso Christl[a]*, and Ruben Kretzschmar[a]

[a]Institute of Biogeochemistry and Pollutant Dynamics, Department of Environmental Systems Science, ETH Zurich, Universitätstrasse 16, CHN, 8092 Zurich, Switzerland

[b]Geomicrobiology Group, Centre for Applied Geosciences (ZAG), University of Tübingen, Hölderlinstrasse 12, D-72074, Tübingen, Germany

*corresponding author, email: iso.christl@env.ethz.ch

Table of Contents

1. Saturation indices

Table S1: Saturation indices for potential minerals forming in Mössbauer and XAS samples at the beginning of anoxic equilibration.

	Clay conc. (g/L)	pH	[Fe^{2+}] (mM)	[Ca^{2+}] (mM)	[Cl^-] (mM)	Sat. Index[a] $Fe(OH)_2$ (am)	Sat. Index[a] $Fe(OH)_2$ (c)	Sat. Index[a] $CaCO_3$	Sat. Index[a] $Ca(OH)_2$
Mössbauer experiments	1	7.0	0.05	10	20.1	**-4.08**	**-3.48**	**-20.99**	**-11.00**
Mössbauer experiments	1	8.2	0.05	10	20.1	**-1.69**	**-1.09**	**-18.59**	**-8.60**
Mössbauer experiments	1	7.3	0.5	10	21.0	**-2.48**	**-1.88**	**-20.40**	**-10.40**
Mössbauer experiments	1	7.7	0.5	10	21.0	**-1.69**	**-1.09**	**-19.60**	**-9.60**
XAS experiments	5	7.0	0.25	50	100.5	**-3.58**	**-2.98**	**-20.51**	**-10.52**
XAS experiments	5	8.1	0.25	50	100.5	**-1.39**	**-0.79**	**-18.31**	**-8.32**
XAS experiments	5	7.2	2.5	50	105.0	**-2.19**	**-1.59**	**-20.12**	**-10.12**
XAS experiments	5	8.1	2.5	50	105.0	**-0.39**	**0.21**	**-18.32**	**-8.32**

[a] Saturation Index = (log IAP – log K_{sp}), IAP (= Ion activity product), K_{sp} (= Stoichiometric solubility product).

Note: a 100% N_2 atmosphere is assumed for all calculations.

2. Protocols to ensure anoxic conditions

Due to the oxygen sensitivity of Fe^{2+}, all sorption experiments and XAS sample preparation were performed under strictly anoxic conditions. All experiments were conducted in an anoxic glovebox with a 100% N_2 atmosphere, equipped with copper catalyst (MBraun) attached to a fan box to scavenge traces of O_2. A O_2-meter was used to monitor the oxygen level during experiments. The O_2-meter reading remained at 0.1 ppm during the entire experimental period. Water used for sample and reagent preparation was boiled and purged with pure nitrogen gas for at least 3 hours outside the glovebox and then transferred inside to cool down and degassed for at least 24 hours before use. All sample containers were wrapped in aluminum foil to minimize any potential photochemical redox reactions. All labware used in the experiments, including bottles, tubes, filters, syringes, and pipette tips, were brought into the glovebox at least one day before use to remove adsorbed oxygen. All batch experiments were prepared in an anoxic glove box from a stock clay suspension (25 g clay/L), which was equilibrated for 7 days in the glovebox.

3. Amount of sorbed Fe^{2+} in samples used for solid phase analysis

Table S2: Percentages of Fe^{2+} sorbed to Syn-1 in samples prepared for solid phase analysis. Iron-to-clay ratios of 0.05 (low Fe-load) and 0.5 mol Fe/kg clay (high Fe-load) were used. All samples were equilibrated for 1 day or 30 days under anoxic conditions. Oxic samples were exposed to O_2 for 1 day after anoxic equilibration. Samples were sorted in samples equilibrated at pH ~7 or ~8 under anoxic conditions. The pH measured at the end of the equilibration period for each sample is given in Table S3.

XAS analysis		**Low Fe-load**		**High Fe-load**	
	Equilibration time (anoxic period)	Anoxic target pH 7	Anoxic target pH 8	Anoxic target pH 7	Anoxic target pH 8
anoxic	1 day	22.0	88.0	27.0	83.0
oxic	1 day	62.8	99.9	36.1	87.0
anoxic	30 days	27.9	92.8	30.4	85.0
oxic	30 days	68.8	99.9	38.0	89.0
Mössbauer analysis		**Low Fe-load**		**High Fe-load**	
	Equilibration time (anoxic period)	Anoxic target pH 7	Anoxic target pH 8	Anoxic target pH 7	Anoxic target pH 8
anoxic	1 day	50.9	79.6	46.3	74.0
oxic	1 day			54.3	99.5

4. pH changes after oxidation

Table S3: pH values of Fe^{2+} sorption batch experiment with Syn-1 (~5 g/L) as measured after equilibration. Iron-to-clay ratios of 0.05 (low Fe-load) and 0.5 mol Fe/kg clay (high Fe-load) were used. At the beginning of the sorption experiments, pH values were adjusted to ~7 and ~8, respectively, as indicated in the header of each column. All samples were equilibrated for 1 day or 30 days under anoxic conditions. Oxic samples were exposed to ambient air for 1 day after anoxic equilibration.

XAS analysis		**Low Fe-load**		**High Fe-load**	
	Equilibration time (anoxic period)	Anoxic target pH 7	Anoxic target pH 8	Anoxic target pH 7	Anoxic target pH 8
anoxic	1 day	7.0	8.1	7.2	8.1
oxic	1 day	5.9	7.3	4.8	5.0
anoxic	30 days	7.0	8.0	6.8	7.6
oxic	30 days	5.6	7.2	4.7	5.0
Mössbauer analysis		**Low Fe-load**		**High Fe-load**	
	Equilibration time (anoxic period)	Anoxic target pH 7	Anoxic target pH 8	Anoxic target pH 7	Anoxic target pH 8
anoxic	1 day	7.0	8.2	7.3	7.7
oxic	1 day			5.1	5.6

5. Fe XANES absorbance for 1 day equilibration samples

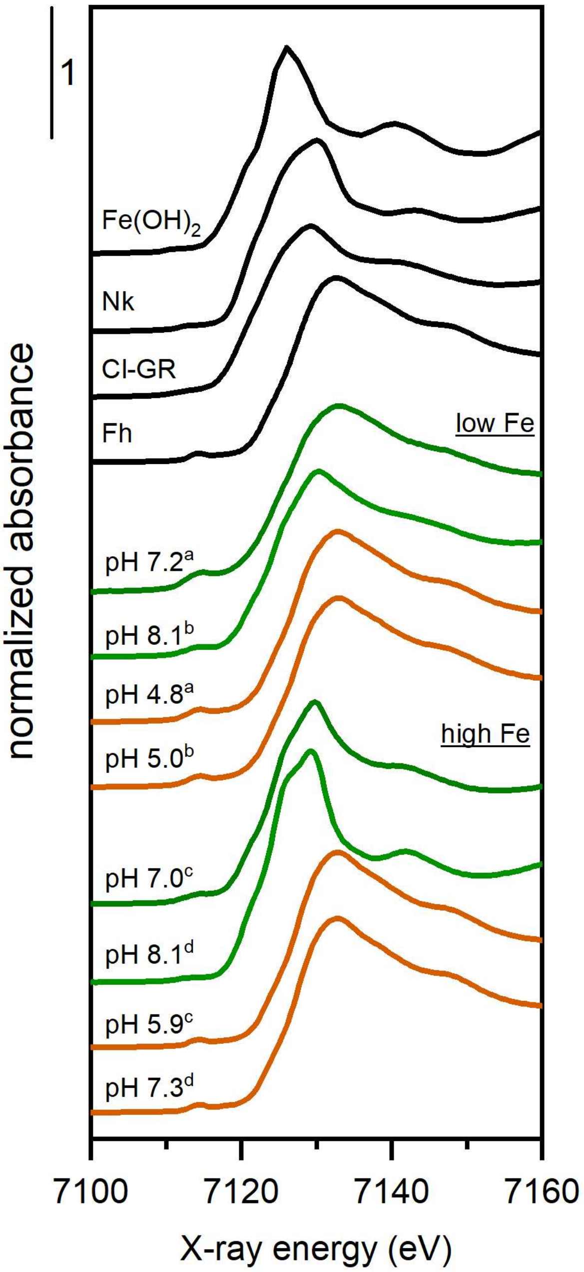

Figure S1: Normalized Fe K-edge XANES spectra of Fe^{2+} sorption samples in which Syn-1 (5 g/L) was reacted with low (0.25 mM) or high (2.5 mM) Fe^{2+} concentrations at pH ~7 or ~8. Sorption samples were equilibrated for 1 day under anoxic conditions (green lines) and subsequently oxidized for 1 day (orange lines). Superscripts (a–d) indicate the corresponding pairs of anoxic and oxidized samples. Selected reference spectra of solid phases containing Fe(II) and/or Fe(III) are shown for comparison (abbreviations: Nk= nikischerite, Cl-GR= chloride green rust, Fh= ferrihydrite). Displayed pH values correspond to the pH measured at the end of the equilibration period for each sample.

6. Pourbaix diagrams for iron and hydrogen

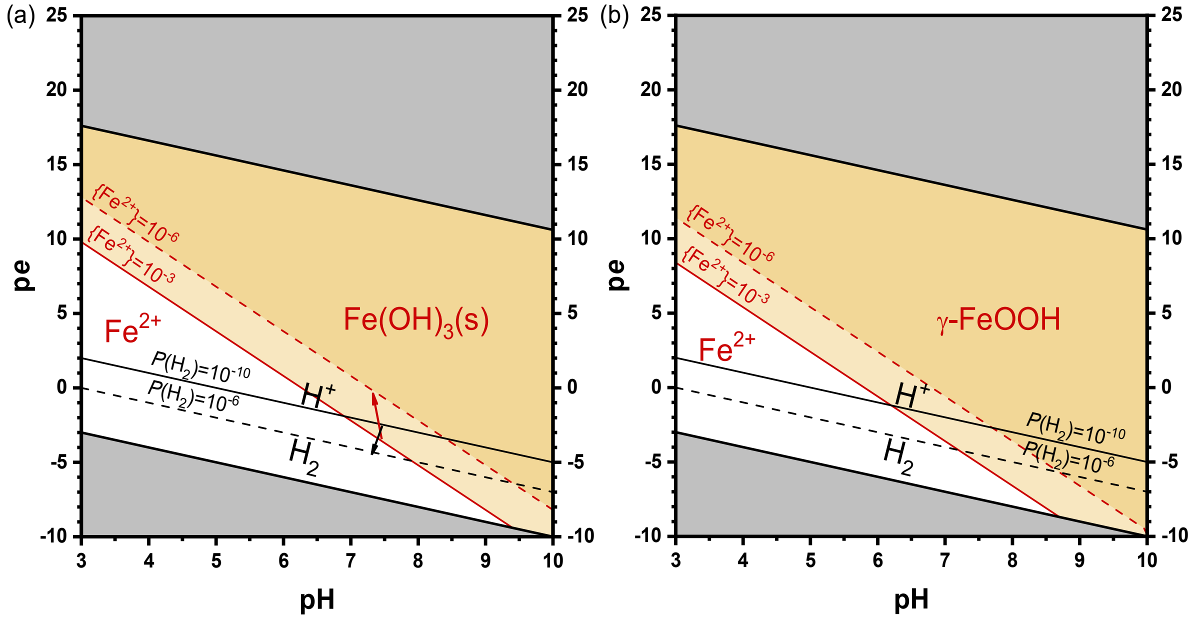

Figure S2: Pourbaix diagrams of iron (red colour) and hydrogen ($H^+ + e^- \rightleftharpoons ½H_2$, logK=0.0, black colour) assuming (a) poorly crystalline $Fe(OH)_3$ ($Fe(OH)_3 + 3H^+ + e^- \rightleftharpoons Fe^{2+} + 3H_2O$, logK=15.8) and (b) γ-FeOOH (lepidocrocite; $FeOOH + 3H^+ + e^- \rightleftharpoons Fe^{2+} + 2H_2O$, logK=14.4), respectively as the solid phase forming during oxidation of Fe^{2+}. Lines were calculated for Fe^{2+} activities of 10^{-3} (solid line) and 10^{-6} (dashed line) and H_2 partial pressures of 10^{-10} (solid line) and 10^{-6}, representing the order of magnitude of the atmospheric H_2 partial pressure (dashed line). Arrows in panel (a) indicate the direction of changes during sample equilibration starting at high Fe^{2+} activities in an atmosphere, which is very low in H_2. Overall, a trend towards lower pH is expected and was also observed in our experiments due to the generation of acidity during iron oxidation.

7. XAS analysis for 30 days equilibration

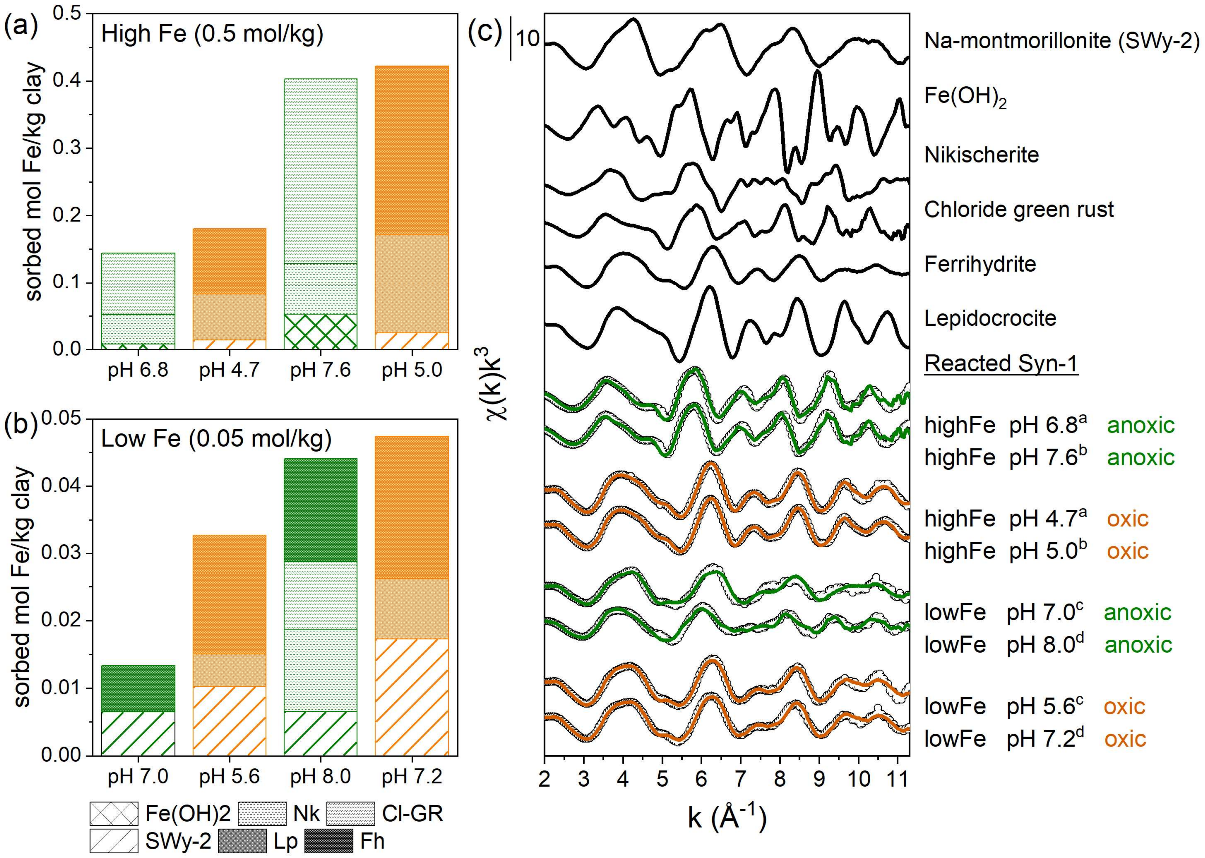

Figure S3: LCF fitting results of Fe K-edge EXAFS spectra of Fe^{2+} sorption samples equilibrated for 30 days under anoxic conditions (green lines) and subsequently oxidized for 1 day (orange lines) and relevant references: (a,b) Absolute fractions of Fe references obtained by linear combination fitting of k^3-weighted Fe K-edge EXAFS spectra for Fe^{2+} sorbed on Syn-1. Green colours refer to anoxic samples and orange colours to oxidized samples. Results are depicted for samples with high Fe-loadings (0.5 mol Fe/kg clay) (a,c) and low Fe-loadings (0.05 mol Fe/kg clay) (b,c). The fits were performed over a k-range of 2–11.3 $Å^{-1}$ (k-weight =3) with no fit constraints. The initial fit fractions (70.9–146.2%) were recalculated to 100% and are reported in Table S11 and S12. Abbreviations: Nk= nikischerite, Cl-GR= chloride green rust, Lp= lepidocrocite, Fh= ferrihydrite). (c) k^3-weighted χ spectra of references (line): SWy-2, $Fe(OH)_2$, nikischerite, chloride green rust, ferrihydrite, and lepidocrocite are shown together with the k^3-weighted χ spectra (open circles) of 30 days equilibrated samples with corresponding fit. Displayed pH values correspond to the pH measured at the end of the equilibration period for each sample. Superscript (a–d) indicate the corresponding pairs of anoxic and oxidized samples.

8. Percentage of Fe sorbed by oxidation of dissolved Fe

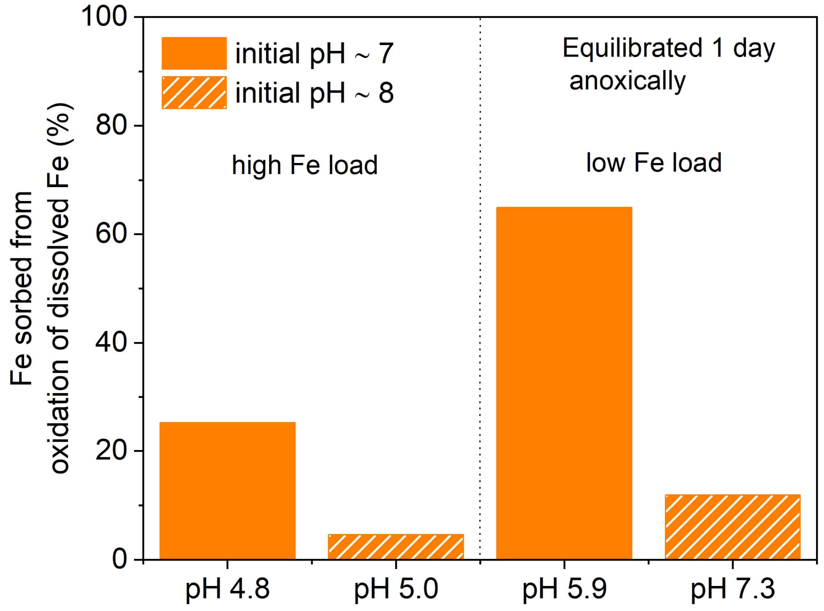

Figure S4: Percentages of Fe sorbed in re-aerated samples that might have formed by direct oxidation of dissolved Fe remaining in solution after anoxic equilibration of Fe^{2+} with Syn-1 (~5 g/L) at pH ~7 and ~8 in a 50 mM $CaCl_2$ background. Iron-to-clay ratios were adjusted to 0.05 (low Fe-load) and 0.5 mol/kg (high Fe-load). All samples were equilibrated for 1 day under anoxic conditions and subsequently oxidized for 1 day.

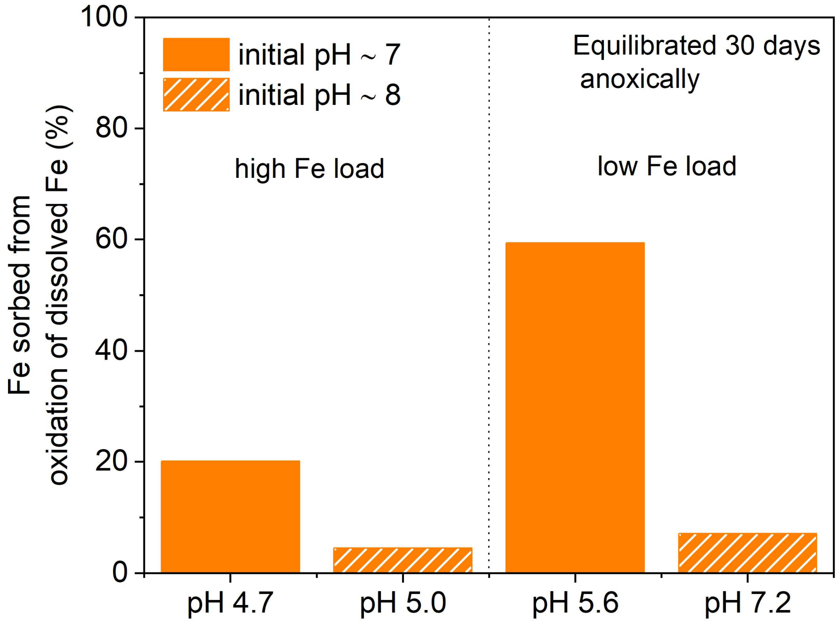

Figure S5: Percentages of Fe sorbed in re-aerated samples that might have formed by direct oxidation of dissolved Fe remaining in solution after anoxic equilibration of Fe^{2+} with Syn-1 (~5 g/L) at pH ~7 and ~8 in a 50 mM $CaCl_2$ background. Iron-to-clay ratios were adjusted to 0.05 (low Fe-load) and 0.5 mol/kg (high Fe-load). All samples were equilibrated for 30 days under anoxic conditions and subsequently oxidized for 1 day.

9. Silicon release during batch experiments

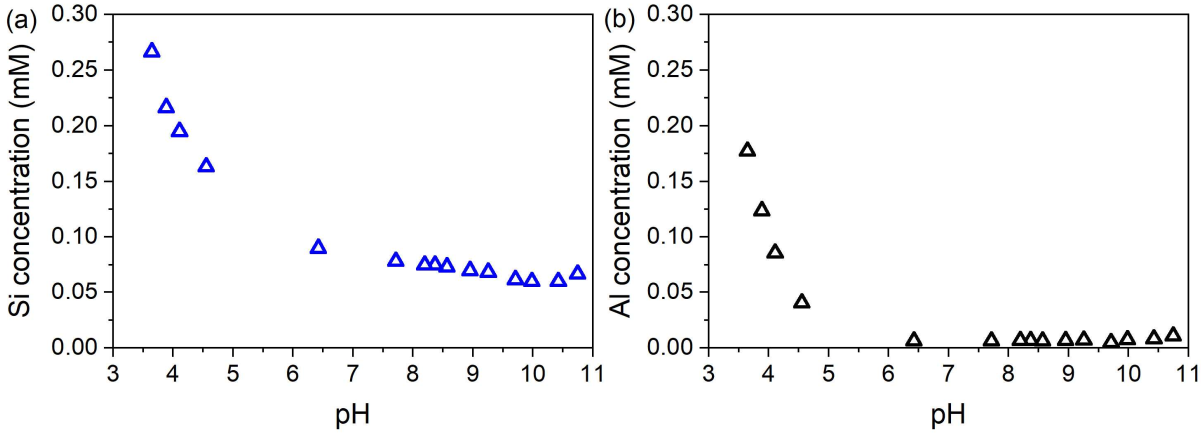

Figure S6: Si (a) and Al (b) released from Syn-1 (~5 g/L) in 50 mM $CaCl_2$ as measured after 1 day equilibration.

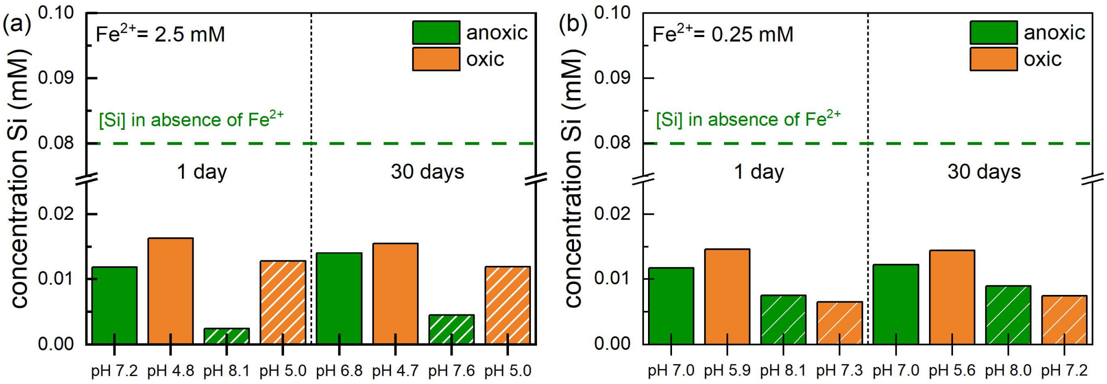

Figure S7: Si released from Syn-1 (~5 g/L) during Fe^{2+} sorption experiments at pH ~7 and ~8 in 50 mM $CaCl_2$. Iron-to-clay ratios were adjusted to (a) 0.5 mol/kg (high Fe-loading) and (b) 0.05 mol/kg (low Fe-loading). All samples were equilibrated for 1 day or 30 days under anoxic conditions and oxic samples were oxidized 1 day after anoxic equilibration. The average Si release from Syn-1 in the pH range 6–10 is indicated by the green dashed line (a, b). Displayed pH values correspond to the pH measured at the end of the equilibration period for each sample.

Table S4: Amounts of sorbed Fe in Fe-phyllosilicates, amount Si re-sorbed upon Fe^{2+} addition and ratio of Fe to Si sorbed for high Fe-loading sorption samples (0.5 mol Fe/kg clay) equilibrated at pH ~7 or ~8. Amounts of sorbed Fe in Fe-phyllosilicates was obtained by linear combination fit of k^3-weighted Fe K-edge EXAFS spectra. Amounts of Si re-sorbed was calculated as the difference of dissolved Si in samples with and without added Fe^{2+}. Displayed pH values correspond to the pH measured at the end of the equilibration period for each sample.

High Fe-load	pH	Equilibration time	SWy-2 (mol Fe/kg clay)	Si sorbed (mol/kg clay)	Fe/Siratio
anoxic[a]	7.2	1 day	0.0117	0.0136	0.85
anoxic[b]	8.1	1 day		0.0155	
oxic[a]	4.8	1 day	0.0159	0.0127	1.25
oxic[b]	5.0	1 day	0.0210	0.0135	1.56
anoxic[a]	6.8	30 days		0.0132	
anoxic[b]	7.6	30 days		0.0129	
oxic[a]	4.7	30 days	0.0145	0.0151	0.96
oxic[b]	5.0	30 days	0.0249	0.0136	1.83

[a, b] *Superscripts indicate the corresponding pairs of anoxic and oxidized samples.*

Table S5: Amounts of sorbed Fe in Fe-phyllosilicates, amount Si re-sorbed upon Fe^{2+} addition and ratio of Fe to Si sorbed for low Fe-loading sorption samples (0.05 mol Fe/kg clay). Amounts of sorbed Fe in Fe-phyllosilicates was obtained by linear combination fit of k^3-weighted Fe K-edge EXAFS spectra. Amounts of Si re-sorbed was calculated as the difference of dissolved Si in samples with and without added Fe^{2+}. Displayed pH values correspond to the pH measured at the end of the equilibration period for each sample.

Low Fe-load	pH	Equilibration time	SWy-2 (mol Fe/kg clay)	Si sorbed (mol/kg clay)	Fe/Si ratio
anoxic[a]	7.0	1 day	0.0049	0.0137	0.36
anoxic[b]	8.1	1 day	0.0058	0.0145	0.40
oxic[a]	5.9	1 day	0.0073	0.0131	0.56
oxic[b]	7.3	1 day	0.0137	0.0147	0.93
anoxic[a]	7.0	30 days	0.0065	0.0136	0.48
anoxic[b]	8.0	30 days	0.0066	0.0142	0.46
oxic[a]	5.6	30 days	0.0103	0.0131	0.78
oxic[b]	7.2	30 days	0.0172	0.0145	1.19

[a, b] *Superscripts indicate the corresponding pairs of anoxic and oxidized samples.*

10. Mössbauer analysis

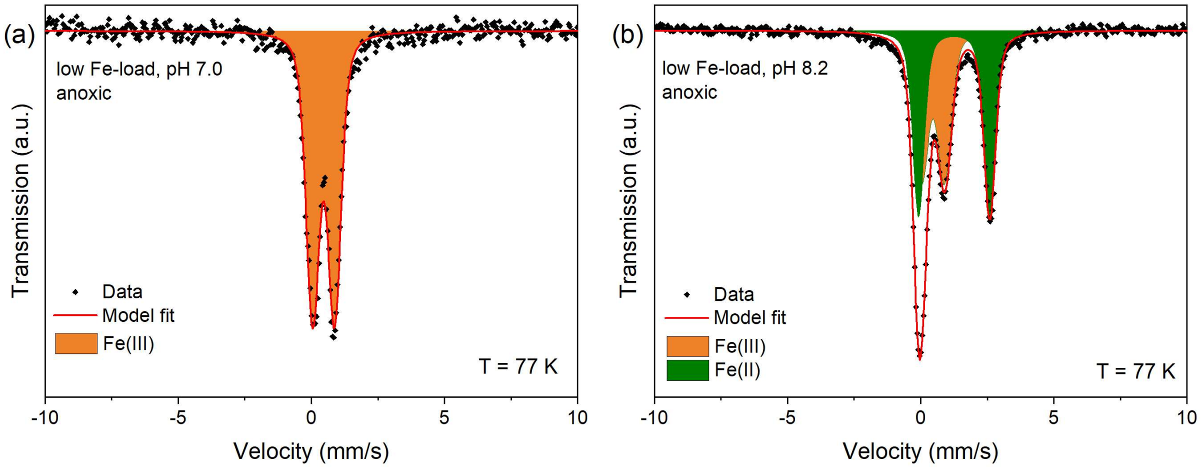

Figure S8: 77 K Mössbauer spectra and fits of selected low Fe-load (0.05 mol Fe/kg clay) samples reacted for 1 day under anoxic conditions. Symbols denote experimental data and red lines represent the model fit. Corresponding fit parameters are summarized in Table S6. The contributions of Fe(II) and Fe(III) to the fit are represented by the green and orange areas, respectively.

Table S6: Fit results for Mössbauer spectra of anoxic and oxic samples with low Fe-loadings (0.05 mol Fe/kg Syn-1) as measured at 77 K. Displayed pH values correspond to the pH measured at the end of the equilibration period for each sample.

Low Fe-load	pH	Oxidation state	δ (mm/s)[a]	ΔE_Q (mm/s)[b]	R.A. (%)[c]
anoxic	7.0	Fe(III)	0.45	0.82	100
anoxic	8.2	Fe(III)	0.46	0.86	47.6
		Fe(II)	1.25	2.66	52.4
High Fe-load	**pH**	**Oxidation state**	**δ (mm/s)[a]**	**ΔE_Q (mm/s)[b]**	**R.A. (%)[c]**
anoxic	7.3[d]	Fe(III)	0.45	0.82	14.1
		Fe(II)	1.27	2.69	85.9
anoxic	7.7[e]	Fe(III)	0.48	0.81	28.1
		Fe(II)	1.26	2.70	71.9
oxic	5.1[d]	Fe(III)	0.46	0.76	100
oxic	5.6[e]	Fe(III)	0.46	0.79	100

[a] δ, isomer shift. [b] ΔE_Q, quadrupole splitting ($\Delta E_Q = 2\varepsilon$), where ε is quadrupole shift. [c] R.A., Relative abundance. [d, e] *Indicate the corresponding pairs of anoxic and oxidized samples.*

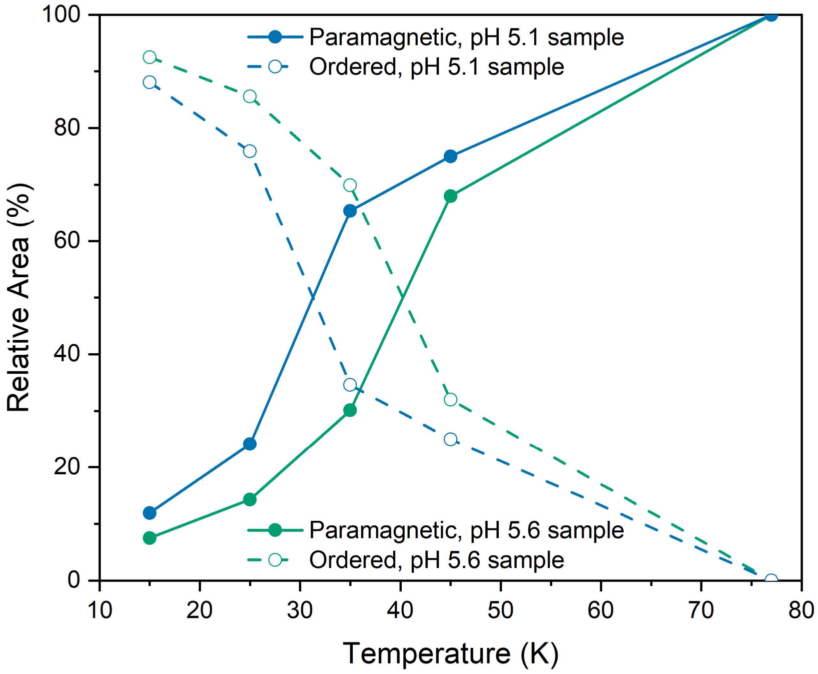

Figure S9: Relative abundance of doublets (solid line) and sextets (dashed line) in ^{57}Fe Mössbauer spectra of two selected oxidized high Fe-load samples, which were equilibrated at pH 7.3 (blue lines) and 7.7 (green lines) under anoxic conditions, as a function of temperature. The blocking temperature is defined as the temperature at which the relative abundance of paramagnetic and magnetically ordered components are equal. For the calculation, the extremely broad doublet and poorly ordered sextets were considered to correspond to the ordered component. Displayed pH values correspond to the pH measured at the end of the oxic equilibration period.

Table S7: Fit results of temperature dependent Mössbauer spectra of oxidized sample with high Fe-loading (0.5 mol Fe/kg Syn-1) equilibrated at pH 7.3 under anoxic conditions and subsequently oxidized.

High Fe-load	T (K)	δ (mm/s)[a]	ΔE_Q (mm/s)[b]	B_{hf} (T)[c]	R.A. (%)[d]
Db[e]	77	0.46	0.76		100
	45	0.47	0.69		75
	45	0.48	1.30		25
Db[e]	35	0.47	0.78		
wDb[f]	35	0.25	4.06		
Db[e]	25	0.47	0.78		24
pSx[g]	25	0.35	0.05	28.5	66
Sx[h]	25	0.39	-0.22	42.1	10
Db[e]	15	0.43	0.77		12
pSx[g]	15	0.60	0.36	31.1	46
Sx[h]	15	0.50	-0.01	43.9	42

[a] δ, isomer shift. [b] ΔE_Q, quadrupole splitting ($\Delta E_Q = 2\varepsilon$), where ε is quadrupole shift. [c] B_{hf}, hyperfine field. [d] R.A., Relative abundance. [e] Db, doublet. [f] wDb, widened doublet. [g] pSx, poorly ordered sextet. [h] Sx, ordered sextet.

Table S8: Fit results of temperature dependent Mössbauer spectra of oxidized high Fe-loading sorption sample equilibrated at pH 7.7 under anoxic conditions and subsequently oxidized.

High Fe-load	**T (K)**	**δ (mm/s)[a]**	**ΔE_Q (mm/s)[b]**	**B_{hf} (T)[c]**	**R.A. (%)[d]**
Db[e]	77	0.46	0.79		100
	45	0.47	0.74		68
	45	0.44	1.49		32
Db[e]	35	0.47	0.78		30
wDb[f]	35	0.40	0.28		70
Db[e]	25	0.46	0.75		14
pSx[g]	25	0.46	0.23	29.4	66
Sx[h]	25	0.42	-0.10	42.4	19
Db[e]	15	0.44	0.73		8
pSx[g]	15	0.38	0.08	33.5	37
Sx[h]	15	0.49	-0.05	44.3	55

[a] δ, isomer shift. [b] ΔE_Q, quadrupole splitting ($\Delta E_Q = 2\varepsilon$), where ε is quadrupole shift. [c] B_{hf}, hyperfine field. [d] R.A., Relative abundance. [e] Db, doublet. [f] wDb, widened doublet. [g] pSx, poorly ordered sextet. [h] Sx, ordered sextet.

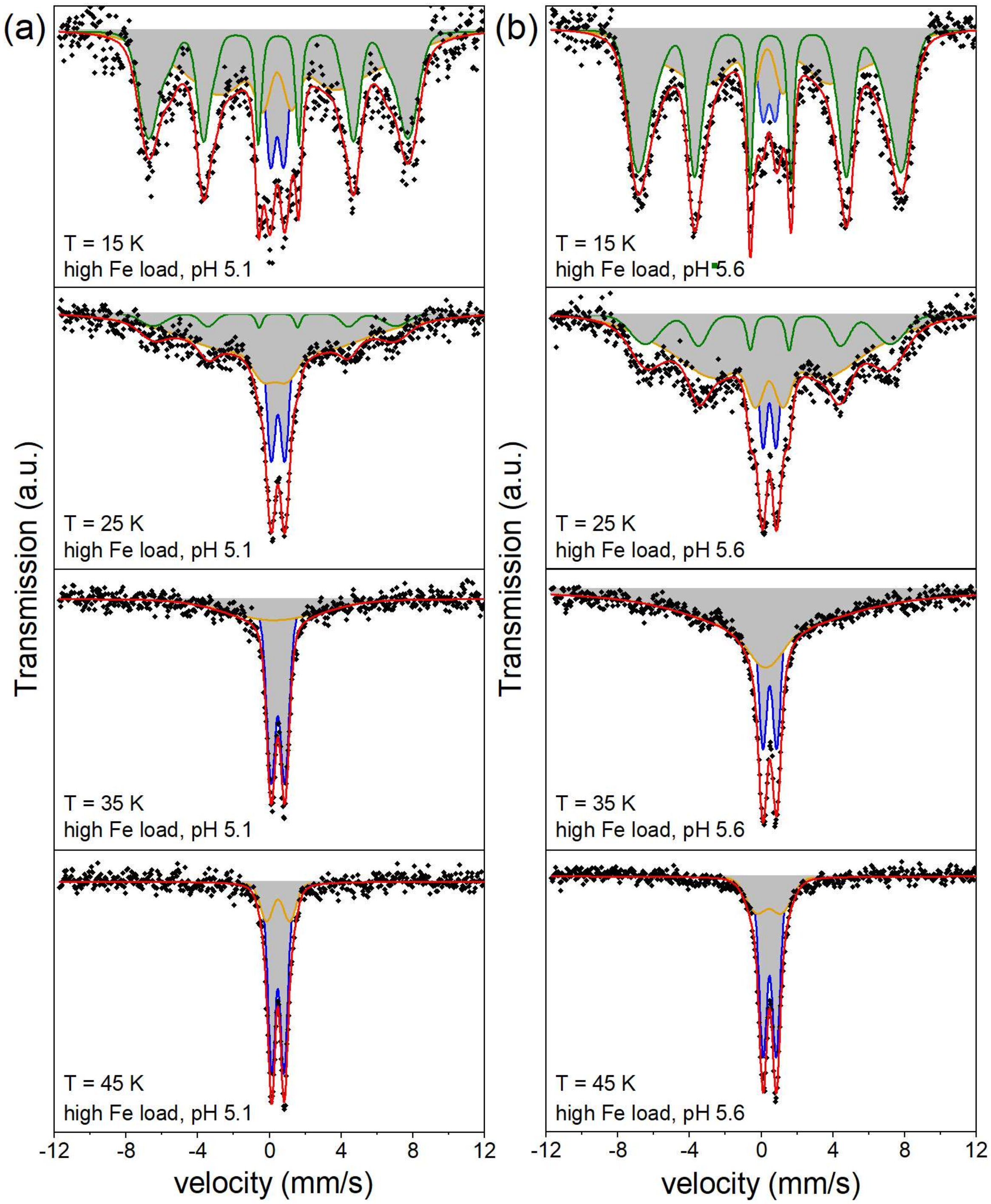

Figure S10: The 15, 25, 35 and 45 K Mössbauer spectra and fits of selected high Fe-loading (0.5 mol Fe/kg clay) samples reacted at pH 7.3 (a) and 7.7 (b) for 1 day under anoxic conditions and subsequently oxidized for 24 hours. Displayed pH values correspond to the pH measured at the end of the oxic equilibration period. Symbols denote experimental data and red lines represent the model fit. The blue (Db), green (Sx) and yellow (pSx) lines represent the different contributions of the fitted doublet (Db) and sextets (S). Corresponding fit parameters are summarized in Table S7 and S8.

11. Fe K-edge X-ray absorption data

Samples for XAS measurements were prepared by homogenizing the dried solids with a mortar and pestle. The homogenized, powder samples were pressed into 13-mm pellets. The pellets were subsequently sealed between Kapton® tape and packed for transport to the synchrotron in two aluminum bags doubly sealed under N_2 gas. Two samples were additionally prepared as oriented clay films and measured with polarized–XAS (α= 10°, 35°, 55°, and 80°). The oriented samples were prepared by collecting the clay on a cellulose filter, separating the solid film from the filters, stacking the solid films, and sealing them between Kapton® tape. All our measurements were conducted at 25 K to avoid beam damage and oxidation of oxygen sensitive samples. For samples with low Fe-loadings (~0.05 mol Fe/kg clay), Fe K-edge (7112 eV) XANES and EXAFS spectra were collected in fluorescence mode using a 36-element array Ge detector (Canberra). High Fe-loading samples (~0.5 mol Fe/kg clay) were measured in transmission mode. For polarized EXAFS spectra of the clay films were recorded at 10°, 35°, 55°, and 80° in fluorescence detection mode.

A Helium cryostat was used to minimize beam-induced redox changes of Fe during measurements. The monochromator (Si(220)) was calibrated to the first-derivative maximum of the K-edge absorption spectrum of a metallic Fe-foil (7112 eV). The Fe-foil was continuously measured to account for small energy shifts (<1 eV) during the sample measurements.

All spectra were energy calibrated, pre-edge subtracted, and post-edge normalized in Athena.[1] In order to identify suitable references for the LCF of Fe K-edge EXAFS spectra of Fe sorption samples (n = 16), principal component analysis (PCA) (k-weight = 3, k-range = 2−11.3 $Å^{-1}$) and target-transformation testing (TT) (k-weight = 3, k-range = 2−11.3 $Å^{-1}$) was performed in SixPack.[2] The results of the PCA analysis performed on k^3-weighted EXAFS spectra are reported for the first six components of the Fe in Tables S9. The IND obtained from PCA analysis of k^3-weighted EXAFS spectra showed that five statistically significant spectral components accounted for 99.5% of spectral variance. Target-transform (TT) was used to identify the importance of specific reference spectra for LCF. The quality of the transformation was evaluated by the empirical SPOIL value[3]: 0−1.5 excellent, 1.5−3 good, 3−4.5 fair, 4.5−6 acceptable, and >6 for an unacceptable reference spectrum. The results of the TT testing are given in Tables S10. From all Fe references tested only the reference with a SPOIL value > 3 were used in LCF analysis. The number of suitable references obtained by TT exceeded the number of PCA components, all suitable references were initially considered in LCF analyses. Because of the sometimes similar EXAFS features in selected references, the numbers of fit references employed exceeded the number of PCA components by one. LCF analyses of k^3-weighted Fe EXAFS spectra were performed over a k-range of 2−11.3 $Å^{-1}$ with the E_0 of all spectra and reference compounds set to 7128 eV (Fe). No constraints were imposed on all LCF fits and initial fit fractions (70.9−146.2%) were recalculated to a compound sum of 100%.

Untreated Swy-2, IMt1, and Nau-2 were used as a Fe(III)-containing clay mineral reference. All clay mineral references were purchased from the Source Clays Repository of the Clay Minerals Society. Swy-2 is a dioctahedral mineral with 3 wt% Fe, IMt1 is a illite with 5 wt% Fe, and Nau-2 is a nontronite with 19.2wt% Fe. Aqueous Fe^{2+} and Fe^{3+} were used as references for outer-sphere adsorption of Fe^{2+} or Fe^{3+} to the clay surface. Lepidocrocite, ferrihydrite, magnetite, maghemite, and goethite were included in LCF analysis as potential Fe(III)-(oxyhydr)oxides forming. Nikischerite was used as a structural reference representing Fe(II)Al(III)-LDH phases which may form in presence of Al-containing phases under anoxic conditions. Both $Fe(OH)_2$ and Cl-GR references were included as potential Fe-phases forming under anoxic conditions.

Table S9: PCA results for k^3-weighted Fe K-edge EXAFS sample spectra (n=16).

Component	**Eigenvalue**	**Variance**	**Cum. Var.**	**IND**
1	69.146	0.669	0.669	0.03568
2	31.028	0.300	0.970	0.00275
3	1.944	0.018	0.988	0.00088
4	0.398	0.003	0.992	0.00073
5	0.330	0.003	0.995	0.00038
6	0.084	0.000	0.996	0.00040

Table S10: Results from the TT analysis using the first five PCA components. (k-range 2–11.3, k^3-weight)

Reference	**χ^2 (-)**	**NSSR (%)[a]**	**SPOIL (-)**
Lepidocrocite γ-FeOOH	151.88	0.0551	0
Na-montmorillonite (Swy-2)	136.82	0.0666	0
Nikischerite[b]	170.96	0.1675	0
$Fe(OH)_2$[b]	1602.49	0.4306	0.54
Fe^{3+} (aq.)[c]	243.74	0.1266	0.62
Chloride green rust[d]	111.14	0.1154	0.96
Ferrihydrite	46.18	0.0479	1.37
Goethite	491.70	0.2991	1.66
Nontronite (Nau-2)	202.47	0.1028	1.72
Illite (IMt1)	101.05	0.0830	2.13
Fe^{2+} (aq.)[c]	472.09	0.4755	2.31
Magnetite Fe_3O_4	1559.02	0.6015	3.55
Maghemite γ-Fe_2O_3	450.18	0.2671	3.60

[a] NSSR Normalized sum of the squared residuals ($=100*\sum(data_i-fit_i)^2 / \sum data_i^2$).

[b] Courtesy of E. Elzinga, Rutgers University.

[c] Courtesy of A. Zitolo, Synchrotron SOLEIL.

[d] Courtesy of T. Borch, Colorado State University

Table S11: Fitted contributions (percentages) of Fe references contributing to samples spectra as obtained by linear combination fit of k^3-weighted Fe K-edge EXAFS spectra for high Fe-loading sorption samples (0.5 mol Fe/kg clay). Abbreviations: SWy-2= Na-montmorillonite, Nk= nikischerite, Cl-GR = chloride green rust, Lp= lepidocrocite, Fh= ferrihydrite). Displayed pH values correspond to the pH measured at the end of the equilibration period.

High Fe-load	**pH**	**Equilibration time**	**SWy-2**	**$Fe(OH)_2$**	**Nk**	**Cl-GR**	**Lp**	**Fh**	**R^{2a}**	**fitted sum**
anoxic[b]	7.2	1 day	9		40	51			0.0840	104.5
anoxic[c]	8.1	1 day		13	25	62			0.0658	146.2
oxic[b]	4.8	1 day	9				25	66	0.0125	102.6
oxic[c]	5.0	1 day	5				36	59	0.0066	102.5
anoxic[b]	6.8	30 days		6	30	64			0.0501	131.7
anoxic[c]	7.6	30 days		13	19	68			0.0506	126.3
oxic[b]	4.7	30 days	8				38	54	0.0119	102.3
oxic[c]	5.0	30 days	6				35	59	0.0060	103.2

[a] R-factor; Normalized sum of squared residuals ($\sum_i (data_i - fit_i)^2 / \sum_i data^2$). [b, c] *Superscripts indicate the corresponding pairs of anoxic and oxidized samples.*

Table S12: Fitted contributions (percentages) of Fe references contributing to samples spectra as obtained by linear combination fit of k^3-weighted Fe K-edge EXAFS spectra for low Fe-loading sorption samples (0.05 mol Fe/kg clay). Abbreviations: SWy-2= Na-montmorillonite, Nk= nikischerite, Cl-GR= chloride green rust, Lp= lepidocrocite, Fh= ferrihydrite). Displayed pH values correspond to the pH measured at the end of the equilibration period.

Low Fe-load	**pH**	**Equilibration time**	**SWy-2**	**$Fe(OH)_2$**	**Nk**	**Cl-GR**	**Lp**	**Fh**	**R^{2a}**	**fitted sum**
anoxic[b]	7.0	1 day	47					53	0.1715	70.9
anoxic[c]	8.1	1 day	14		32	28		26	0.0619	112.5
oxic[b]	5.9	1 day	24				16	60	0.0158	98.3
oxic[c]	7.3	1 day	29				13	58	0.0176	96.9
anoxic[b]	7.0	30 days	49					51	0.0750	79.8
anoxic[c]	8.0	30 days	15		27	23		35	0.0699	114.7
oxic[b]	5.6	30 days	31				15	54	0.0256	102.8
oxic[c]	7.2	30 days	36				19	45	0.0181	96.2

[a] R-factor; Normalized sum of squared residuals ($\sum_i (data_i - fit_i)^2 / \sum_i data^2$). [b, c] I*ndicate the corresponding pairs of anoxic and oxidized samples.*

Shell-fit analyses of the extended X-ray absorption fine structure (EXAFS) spectra were performed in order to obtain information about the short range local coordination environment of Fe. Fourier transforms of k^3-weighted EXAFS spectra were calculated over a k-range of 2–10.5 $Å^{-1}$ (except for anoxic low Fe-loading sample at pH 7, k-range of 2–9.5 $Å^{-1}$) using a Kaiser-Bessel window function and the frequency cut-off parameter, Rbkg, was set to 1.0. The edge-energy, E_0, was defined as the maximum in the first XANES derivatives. Shell-fit analyses of k^3-weighted Fe EXAFS spectra were performed in R-space R + ΔR-range of 1.1−3.2 Å (except for anoxic low Fe-loading sample at pH 7, R + ΔR-range of 1.1–4 Å) using the software Artemis.[1] Theoretical phase-shift and amplitude functions were calculated with FEFF v.6[4, 5] based on the structures of fougerite ($Fe^{2+}{}_4Fe^{3+}{}_2(OH)_{12}[CO_3]\cdot 3H_2O$),[6] goethite (α-FeOOH),[7] greenalite ($Fe_6(Si_4O_{10})(OH)_8$),[8] nikischerite ($NaFeAl_3(SO_4)_2(OH)_{18}(H_2O)_{12}$),[9] and lepidocrocite (γ-FeOOH).[10]

Table S13: Shell-fit parameters determined from Fe K-edge EXAFS data of Fe(II) sorption to Syn-1 under anoxic conditions for 30 days.[a]

	Fe-O									Fe-Fe					
High Fe load	**CN**[b]	**R(Å)**[c]	**σ^2 (Å^2)**[d]							**CN**[b]	**R(Å)**[c]	**σ^2 (Å^2)**[d]	**ΔE_0**[e]	**Red. χ^2**[f]	**R-factor**[g]
pH 6.8	5.3 (0.5)	2.11 (0.01)	0.010 (0.001)							3.6 (0.5)	3.20 (0.01)	0.006 (0.001)	-1.86 (0.83)	121	0.0044
pH 7.6	5.4 (0.5)	2.12 (0.01)	0.010 (0.001)							4.2 (0.6)	3.21 (0.01)	0.007 (0.001)	-0.52 (0.82)	283	0.0043
Low Fe load	**CN**[b]	**R(Å)**[c]	**σ^2 (Å^2)**[d]							**CN**[b]	**R(Å)**[c]	**σ^2 (Å^2)**[d]	**ΔE_0**[e]	**Red. χ^2**[f]	**R-factor**[g]
pH 8.0	4.6 (0.8)	2.05 (0.01)	0.011 (0.002)							1.8 (0.3)	3.15 (0.02)	0.009	1.27 (1.72)	188	0.0246
	Fe-O			Fe-Al			Fe-Si			Fe-Fe					
Low Fe load	**CN**[b]	**R(Å)**[c]	**σ^2 (Å^2)**[d]	**CN**[b]	**R(Å)**[c]	**σ^2 (Å^2)**[d]	**CN**[b]	**R(Å)**[c]	**σ^2 (Å^2)**[d]	**CN**[b]	**R(Å)**[c]	**σ^2 (Å^2)**[d]	**ΔE_0**[e]	**Red. χ^2**[f]	**R-factor**[g]
pH 7.0	4.7 (0.8)	2.02 (0.01)	0.008 (0.002)	1.6 (1.2)	2.82 (0.06)	0.01	0.5 (1.5)	3.0 (0.2)	0.01	1.5 (0.6)	3.47 (0.03)	0.009	-0.55 (1.97)	128	0.0170

[a]The amplitude reduction factor S_0^2 was set to 0.9 based on first shell optimization for all sorption samples (R-range 1.1–2.5 Å). [b]Path degeneracy (coordination number). [c]Mean half path length. [d]Debye–Waller parameter. Debye–Waller parameter was fixed to 0.01 Å^2 for Fe-Al and Fe-Si based on the σ^2 obtained for Fe-Si and Fe-Al path by Soltermann et al.[11] σ^2 (Fe) was fixed to 0.009 Å^2 for Fe-Fe of low Fe-load sorption sample like was fitted for edge-sharing Fe-Fe for low Fe-loading samples. [e]Energy-shift parameter. [f]Fit accuracy; reduced $\chi^2 = (N_{idp}/N_{pts})\sum_i ((data_i - fit_i)/\varepsilon_i)^2 (N_{idp}-N_{var})^{-1}$. N_{idp}, N_{pts} and N_{var} are, respectively, the number of independent points in the model fit (11.2–13.7), the total number of data points (151–171), and the number of fit variables (6–10). ε_i is the uncertainty of the *i*th data point.[g]R-factor; Normalized sum of squared residuals ($\sum_i (data_i - fit_i)^2 / \sum_i data^2$). Note: Parameter uncertainties are given in parentheses. The FT of k^3-weighted EXAFS spectrum of the anoxic low Fe-loading samples at pH 8 was calculated over a k-range of 2–9.5 Å^{-1}. The shell-fit analysis of k^3-weighted Fe EXAFS spectrum of the anoxic low Fe-loading sample at pH 7 was performed in R-space R + ΔR-range of 1.1–4 Å.

Table S14: Shell-fit parameters determined from shell fitting of FT of Fe K-edge EXAFS data for oxic Fe sorption samples which were equilibrated for 1 or 30 days under anoxic conditions and subsequently oxidized for 1 day.[a] *Displayed pH values correspond to the pH measured at the end of the oxic equilibration period.*

		Fe-O			Fe-Fe$_1$			Fe-Fe$_2$					
High Fe-load	**pH**	**CN**[b]	**R(Å)**[c]	**σ^2 (Å^2)**[d]	**CN**[b]	**R(Å)**[c]	**σ^2 (Å^2)**[d]	**CN**[b]	**R(Å)**[c]	**σ^2 (Å^2)**[d]	**ΔE_0**[e]	**Red. χ^2**[f]	**R-factor**[g]
1 day anoxic + 1 day oxic	4.8	6.0 (0.7)	1.99 (0.0)	0.009 (0.001)	3.1 (0.4)	3.07 (0.01)	0.009	1.0 (0.5)	3.43 (0.04)	0.009	-1.77 (1.33)	218	0.0052
1 day anoxic + 1 day oxic	5.0	5.8 (0.6)	1.99 (0.01)	0.010 (0.001)	3.7 (0.4)	3.07 (0.01)	0.009	1.0 (0.5)	3.42 (0.03)	0.009	-2.20 (1.20)	811	0.0044
30 days anoxic + 1 day oxic	4.7	5.4 (0.8)	1.99 (0.01)	0.009 (0.002)	3.7 (0.5)	3.08 (0.01)	0.009	1.7 (0.7)	3.42 (0.03)	0.009	-2.10 (1.72)	333	0.0089
30 days anoxic + 1 day oxic	5.0	5.8 (0.7)	1.99 (0.01)	0.010 (0.001)	3.6 (0.4)	3.07 (0.01)	0.009	1.2 (0.6)	3.42 (0.04)	0.009	-2.42 (1.50)	1823	0.0068

[a] The amplitude reduction factor S_0^2 was set to 0.9 based on first shell optimization for all sorption samples (R 1.1–2.5 Å). [b] Path degeneracy (coordination number). [c] Mean half path length. [d] Debye−Waller parameter. Debye−Waller parameter was fixed to 0.009 Å^2 for Fe-Fe of low Fe-loading sorption sample like was fitted for edge-sharing Fe-Fe for low Fe-loading samples. [e] Energy-shift parameter. [f] Fit accuracy; reduced $\chi^2 = (N_{idp}/N_{pts})\sum_i ((data_i - fit_i)/\varepsilon_i)^2 (N_{idp}-N_{var})^{-1}$. N_{idp}, N_{pts} and N_{var} are, respectively, the number of independent points in the model fit (11.2), the total number of data points (171), and the number of fit variables (8). ε_i is the uncertainty of the i^{th} data point. [g] R-factor; Normalized sum of squared residuals ($\sum_i (data_i - fit_i)^2 / \sum_i data^2$). Notes: Parameter uncertainties are given in parentheses.

Table S15: Shell-fit parameters determined from shell fitting of FT of Fe K-edge EXAFS data for oxic Fe sorption samples which were equilibrated for 1 or 30 days under anoxic conditions and subsequently oxidized for 1 day.[a] *Displayed pH values correspond to the pH measured at the end of the oxic equilibration period.*

		Fe-O			Fe-Fe$_1$			Fe-Fe$_2$					
Low Fe-load	**pH**	**CN**[b]	**R(Å)**[c]	**σ^2 (Å^2)**[d]	**CN**[b]	**R(Å)**[c]	**σ^2 (Å^2)**[d]	**CN**[b]	**R(Å)**[c]	**σ^2 (Å^2)**[d]	**ΔE$_0$**[e]	**Red. χ^2**[f]	**R-factor**[g]
1 day anoxic + 1 day oxic	5.9	5.1 (0.8)	2.00 (0.01)	0.008 (0.001)	2.0 (0.5)	3.07 (0.02)	0.009	1.6 (0.8)	3.44 (0.04)	0.009	-1.36 (1.97)	354	0.0139
1 day anoxic + 1 day oxic	7.3	5.0 (0.7)	1.99 (0.01)	0.008 (0.002)	1.8 (0.4)	3.08 (0.02)	0.009	1.5 (0.6)	3.45 (0.03)	0.009	-1.76 (1.60)	186	0.0093
30 days anoxic + 1 day oxic	5.6	4.9 (0.7)	2.00 (0.01)	0.007 (0.002)	1.9 (0.5)	3.09 (0.02)	0.009	2.1 (0.8)	3.45 (0.03)	0.009	-0.62 (1.76)	226	0.0117
30 days anoxic + 1 day oxic	7.2	5.1 (0.7)	2.00 (0.01)	0.007 (0.002)	1.8 (0.5)	3.09 (0.02)	0.009	1.5 (0.2)	3.45 (0.01)	0.009	-1.41 (1.67)	201	0.0106

[a]The amplitude reduction factor S_0^2 was set to 0.9 based on first shell optimization for all sorption samples (R 1.1–2.5 Å). [b]Path degeneracy (coordination number). [c]Mean half path length. [d]Debye–Waller parameter. Debye–Waller parameter was fixed to 0.009 Å^2 for Fe-Fe of low Fe-loading sorption sample like was fitted for edge-sharing Fe-Fe for low Fe-loading samples. [e]Energy-shift parameter. [f]Fit accuracy; reduced $\chi^2 = (N_{idp}/N_{pts})\sum_i ((data_i - fit_i)/\varepsilon_i)^2 (N_{idp}-N_{var})^{-1}$. N_{idp}, N_{pts} and N_{var} are, respectively, the number of independent points in the model fit (11.2), the total number of data points (171), and the number of fit variables (8). ε_i is the uncertainty of the i^{th} data point. [g]R-factor; Normalized sum of squared residuals $(\sum_i (data_i - fit_i)^2 / \sum_i data^2)$. Notes: Parameter uncertainties are given in parentheses.

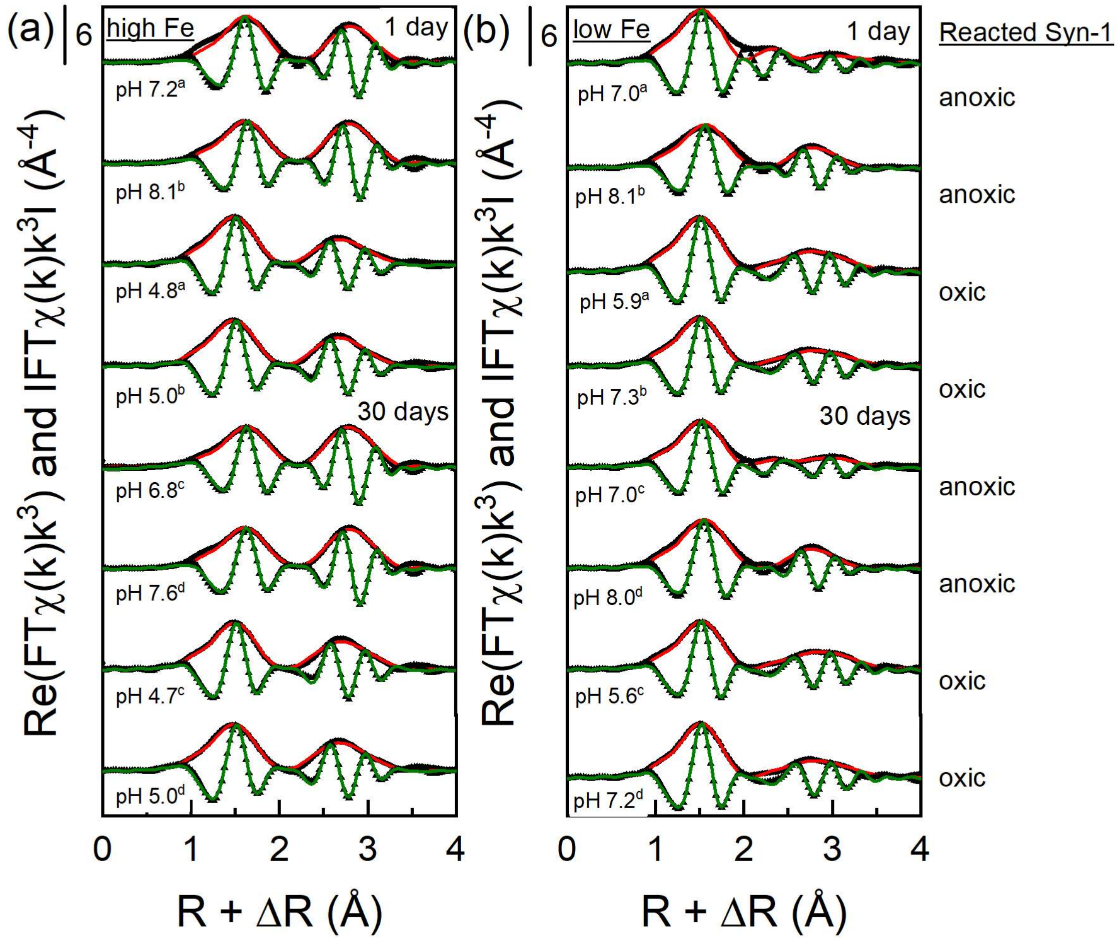

*Figure S11: Fourier transform real parts and magnitudes of the Fe K-edge EXAFS spectra of selected samples with corresponding shell fit. Points indicate experimental data and dotted lines show the model fits. The fits were performed over a R-range of 1.1–3.2 Å (k-weight =3) except for the anoxic low Fe-loading samples equilibrated at pH 7 for which fits were performed over a R-range of 1.1–4.0 Å. The corresponding EXAFS parameters are reported in Tables 2 and, S13–15. Displayed pH values correspond to the pH measured at the end of the equilibration period. Superscripts (a–*d*) indicate the corresponding pairs of anoxic and oxidized samples.*

12. Alternative Fe K-edge EXAFS shell fits of anoxic high Fe-loading samples

Three nucleation products have been reported to form upon iron uptake on clay minerals under anoxic conditions and high Fe-load, namely β-Fe(OH)$_2$, Fe-Al LDH and Fe-phyllosilicate. Due to the similar or even identical crystallographic position of Fe^{2+} and Al^{3+} in LDH phases it is difficult to unequivocally differentiate these two atoms. Additionally, constructive interferences from Si^{4+} atoms in greenalite, which is found at slightly larger crystallographic positions than Fe^{2+} and Al^{3+}, could occur. Therefore, three models for the shell fitting of Fe-loading anoxic samples were suggested, namely:

Model 1: Fe-O and Fe-Fe backscattering paths included in fit.

Model 2: Fe-O, Fe-Fe and Fe-Al backscattering paths included in fit.

Model 3: Fe-O, Fe-Fe and Fe-Si backscattering paths included in fit.

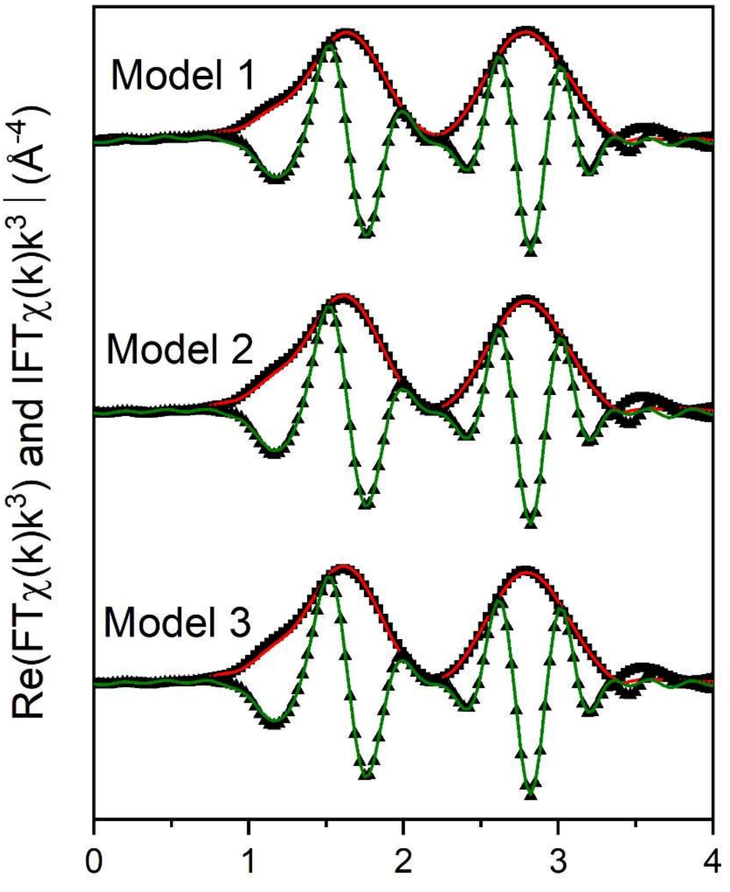

Figure S12: Fourier transform real parts and magnitudes of the Fe K-edge EXAFS spectra of selected sample (high Fe-loading anoxic sample equilibrated at pH 8.1 for 1 day) with model shell fits 1, 2 and 3. Points indicate experimental data and lines show the model fits. The shell fits were performed over a R-range of 1.1–3.2 Å (k-weight =3). The corresponding EXAFS parameters are reported in Table S16.

Table S16: Shell-fit parameters determined by three different fitting models (model 1, 2 and 3) of Fe K-edge EXAFS data of high Fe-loading anoxic sample equilibrated at pH 8.1 for 1 day.[a]

	Fe-O			Fe-Fe			Fe-Al					
Model 1	**CN**[b]	**R(Å)**[c]	**σ^2 (Å^2)**[d]	**CN**[b]	**R(Å)**[c]	**σ^2 (Å^2)**[d]				**ΔE_0**[e]	**Red. χ^2**[f]	**R-factor**[g]
	6.0	2.12	0.009	4.5	3.20	0.007				-1.53	235	0.0032
	(0.5)	(0.01)	(0.001)	(0.5)	(0.01)	(0.001)				(0.72)		
Model 2	**CN**[b]	**R(Å)**[c]	**σ^2 (Å^2)**[d]	**CN**[b]	**R(Å)**[c]	**σ^2 (Å^2)**[d]	**CN**[b]	**R(Å)**[c]	**σ^2 (Å^2)**[d]	**ΔE_0**[e]	**Red χ^2**[f]	**R-factor**[g]
	5.9	2.11	0.009	6.5	3.21	0.008	2.7	3.30	0.005	-2.68	322	0.0013
	(0.6)	(0.01)	(0.001)	(1.9)	(0.02)	(0.001)	(2.2)	(0.06)	(0.008)	(1.27)		
	Fe-O			Fe-Fe			Fe-Si					
Model 3	**CN**[b]	**R(Å)**[c]	**σ^2 (Å^2)**[d]	**CN**[b]	**R(Å)**[c]	**σ^2 (Å^2)**[d]	**CN**[b]	**R(Å)**[c]	**σ^2 (Å^2)**[d]	**ΔE_0**[e]	**Red. χ^2**[f]	**R-factor**[g]
	5.9	2.12	0.009	5.4	3.20	0.007	1.70	3.19	0.010	-2.34	153	0.0016
	(0.4)	(0.01)	(0.001)	(0.3)	(0.01)	(0.002)	(0.9)	(0.06)	(0.100)	(0.72)		

[a]The amplitude reduction factor S_0^2 was set to 0.9 based on first shell optimization for all sorption samples (R 1.1–2.5 Å). [b]Path degeneracy (coordination number). [c]Mean half path length. [d]Debye–Waller parameter. [e]Energy-shift parameter. [f]Fit accuracy; reduced $\chi^2 = (N_{idp}/N_{pts})\sum_i ((data_i - fit_i)/\varepsilon_i)^2 (N_{idp}-N_{var})^{-1}$. N_{idp}, N_{pts} and N_{var} are, respectively, the number of independent points in the model fit (11.2), the total number of data points (171), and the number of fit variables (7–10). ε_i is the uncertainty of the *i*th data point. [g]R-factor; Normalized sum of squared residuals ($\sum_i (data_i - fit_i)^2 / \sum_i data^2$). Notes: Parameter uncertainties are given in parentheses.

13. F-test for anoxic low Fe-loading sample (pH 7)

To test if the inclusion of backscattering paths into a fit model significantly improves the fit quality, we employed F-tests based on crystallographic R-factors (square root of R-factors calculated in Artemis[1, 12, 13] to compare different models. The confidence level, α, that a model (with the inclusion of additional backscattering path) yielded a statistically better fit than the original model was calculated according to eq. 1:

$$\alpha = P\left(F > F_{b,n-m,\alpha}\right) = 1 - I_x\left[\frac{n-m}{2}, \frac{b}{2}\right] \qquad (1)$$

Here, P represents the probability [%], $I_x\left[\frac{n-m}{2}, \frac{b}{2}\right]$ is the incomplete regularized beta function, the parameter x is given by $x = \left(\frac{R_a}{R_b}\right)^2$, b is the dimension of the hypothesis, which is defined as the difference in the degrees of freedom between the fits ($N_{var,b}$ - $N_{var,a}$), n is the number of independent data points as calculated by the Stern's rule,[14] and m is the number of fit parameters.[15] Parameter x represents the ratio of the crystallographic R-factors determined for model a (R_a) and model b (R_b).

The addition of backscattering paths to the model for the Fe K-edge EXAFS shell of the low Fe-loading anoxic samples equilibrated at pH 7.0 were compared using F-tests. Each model contained following backscattering paths:

Model 1: Fe-O and double corner-sharing Fe-Fe backscattering path
Model 2: Fe-O, double corner-sharing Fe-Fe backscattering path and Fe-Al
Model 3: Fe-O, Fe-Al, double corner-sharing Fe-Fe and Fe-Si backscattering scattering path

The test results are summarized in Table S17. Model 3 and 4 significantly improve the fits because α were above or close to the required 67%.[15] Therefore, the inclusion of a Fe-Al and Fe-Si backscattering path is supported by these results.

Table S17: Statistical parameters of Fe K-edge EXAFS shell fits and F-test results. Comparison of three models adding backscattering path for Fe-Fe and Fe-Si.

	R-factor[a]	**N_{idp}**[b]	**N_{var}**[c]	**α [%]**[d]
Model 1	0.0848	13.7	7	
Model 2 (adding Fe-Al path)	0.0470	13.7	8	97
Model 3 (adding Fe-Si path)	0.0361	13.7	10	62

[a]Defined as $\sum_i(data_i\text{-}fit_i)^2 / \sum_i data^2$ (Artemis output). [b]N_{idp} is the number of independent data points. [c]N_{var} is the number of fit parameters. [d]Probability that model 2 yields a statistically better fit than model 1 and model 3 yields a statistically better fit than model 2.

14. Wavelet transformation

Wavelet transformation (WT) of k^3-weighted data were performed using the Fortran version of the HAMA Wavelet Transform software developed by Funke et al.[16] High-resolution WTs of Fe (R + ΔR-range = 2.3–3.6 Å; $\kappa = 5.8$, $\sigma = 1$) were compared with the WT of the second shell of reference compounds (ferrous hydroxide, nikischerite, chloride green rust, SWy-2) (see Figure S11 and S12).

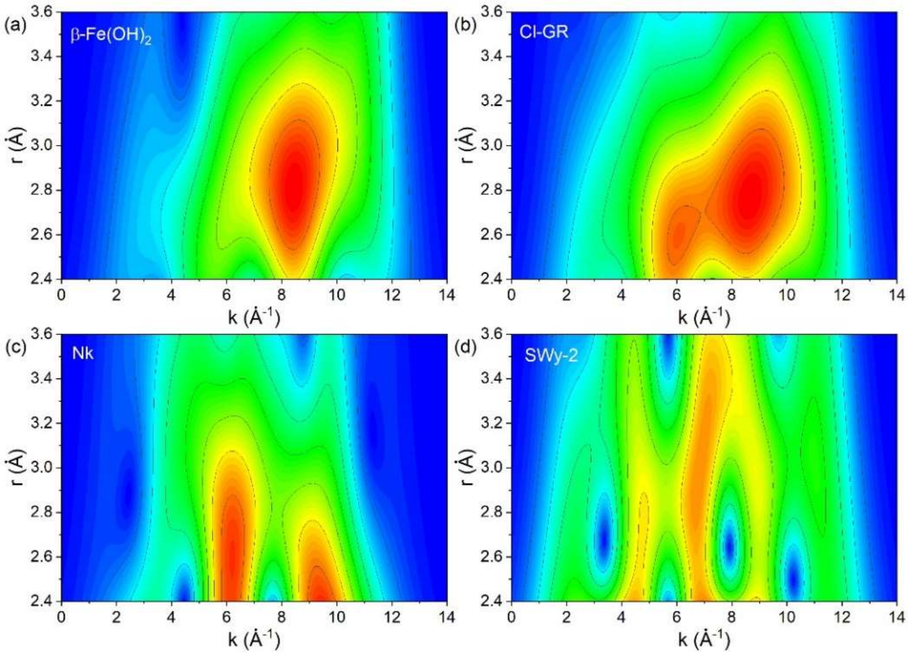

Figure S13: High-resolution WT analyses of the second over the whole spectral range (R + ΔR 2.3–3.6 Å ;κ = 5.8, σ = 1) for reference compounds, (a) β-Fe(OH)$_2$, (b) chloride green rust, (c) nikischerite and (d) SWy-2.

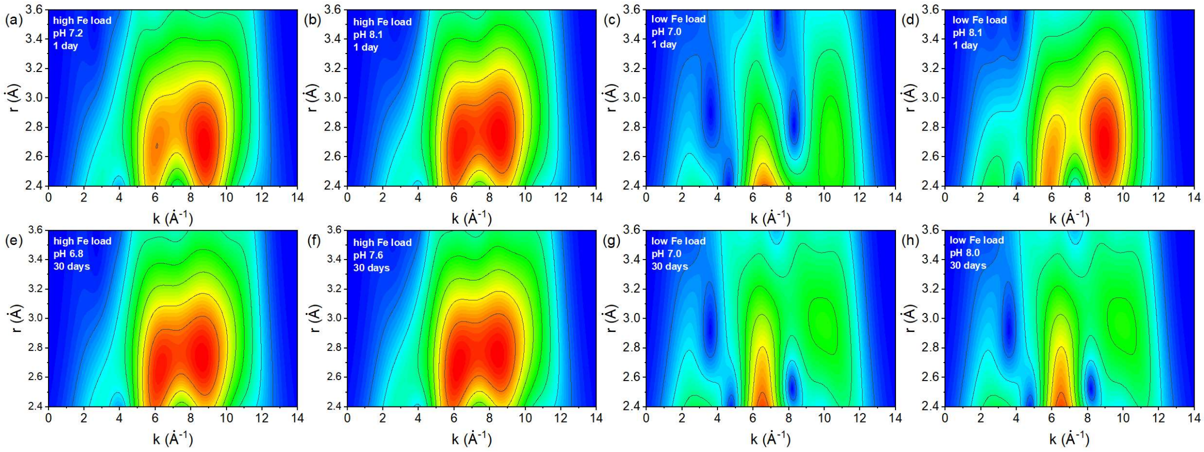

Figure S14: High-resolution WT analyses of the second over the whole spectral range (R + ΔR 2.3 – 3.5 Å ;κ = 5.8, σ = 1) for anoxic sorption sample with (a) high Fe-loading at pH 7.2 equilibrated for 1 day, (b) high Fe-loading at pH 8.1 equilibrated for 1 day, (c) low Fe-loading at pH 7.0 equilibrated for 1 day and (d) low Fe-loading at pH 8.1 equilibrated for 1 day, (e) high Fe-loading at pH 6.8 equilibrated for 30 days, (f) high Fe-loading at pH 7.6 equilibrated for 30 days, (g) low Fe-loading at pH 7.0 equilibrated for 30 days and (h) low Fe-loading at pH 8.0 equilibrated for 30 days.

15. Multiple scattering paths

Selected sorption samples were tested if including multiple scattering (MS) paths significantly improved the fit. Only sorption samples for which the LCF of the EXAFS spectra, ferrihydrite as major phase fitted, were tested. However, MS paths were not tested for low Fe-loading anoxic samples as the LCF of their EXAFS spectra gave unsatisfactory fit. The basic model included a Fe-O path, and two Fe-Fe paths. This model was compared to the basic model including a Fe-O-O triangular MS path (see Table S18)). MS path Fe-O-O was not implemented in our fit model as including this path decreased the reduced χ^2-values less than a factor two (see Kelly et al., 2008 for details).[17]

Table S18: Shell-fit parameters determined from shell fitting of FT of Fe K-edge EXAFS data for oxic Fe sorption samples which were equilibrated for 1 day under anoxic conditions and subsequently oxidized for 1 day. [a]The model with the inclusion of a triangular Fe–O–O multiple scattering path is compared to the model including no MS paths. Displayed pH values correspond to the pH measured at the end of the oxic equilibration period.

		Fe-O			Fe-Fe$_1$			Fe-Fe$_2$					
High Fe-loading	**pH**	**CN[b]**	**R(Å)[c]**	**σ^2 (Å^2)[d]**	**CN[b]**	**R(Å)[c]**	**σ^2 (Å^2)[d]**	**CN[b]**	**R(Å)[c]**	**σ^2 (Å^2)[d]**	**ΔE_0[e]**	**Red. χ^2[f]**	**R-factor[g]**
1 day anoxic	4.8	6.0	1.99	0.009	3.1	3.07	0.009	1.0	3.43	0.009	-1.77	218	0.0052
+ 1 day oxic		(0.7)	(0.01)	(0.001)	(0.4)	(0.01)		(0.5)	(0.04)		(1.33)		
	4.8	5.5	1.99	0.009	2.9	3.07	0.009	1.0	3.43	0.009	-2.24	144	0.0033
incl. Fe-O-O path[h]		(0.5)	(0.01)	(0.001)	(0.3)	(0.01)		(0.5)	(0.04)		(1.06)		
1 day anoxic	5.0	5.8	1.99	0.010	3.7	3.07	0.009	1.0	3.42	0.009	-2.20	811	0.0044
+ 1 day oxic		(0.6)	(0.01)	(0.001)	(0.4)	(0.01)		(0.5)	(0.03)		(1.20)		
	5.0	5.8	1.99	0.009	3.7	3.07	0.009	1.1	3.42	0.009	-2.24	647	0.0035
incl. Fe-O-O path[h]		(0.6)	(0.01)	(0.001)	(0.3)	(0.01)		(0.4)	(0.03)		(1.06)		
Low Fe-loading	**pH**	**CN[b]**	**R(Å)[c]**	**σ^2 (Å^2)[d]**	**CN[b]**	**R(Å)[c]**	**σ^2 (Å^2)[d]**	**CN[b]**	**R(Å)[c]**	**σ^2 (Å^2)[d]**	**ΔE_0[e]**	**Red. χ^2[f]**	**R-factor[g]**
1 day anoxic	5.9	5.1	2.00	0.008	2.0	3.07	0.009	1.6	3.44	0.009	-1.36	354	0.0139
+ 1 day oxic		(0.8)	(0.01)	(0.001)	(0.5)	(0.02)		(0.8)	(0.04)		(1.97)		
	5.9	5.0	1.99	0.008	1.7	3.07	0.009	2.0	3.44	0.009	-1.49	279	0.0110
incl. Fe-O-O path[h]		(0.7)	(0.01)	(0.002)	(0.5)	(0.2)		(0.7)	(0.03)		(1.66)		
1 day anoxic	7.3	5.0	1.99	0.008	1.8	3.08	0.009	1.5	3.45	0.009	-1.76	185.58	0.0093
+ 1 day oxic		(0.7)	(0.01)	(0.002)	(0.4)	(0.02)		(0.6)	(0.03)		(1.60)		
	7.3	5.0	1.993	0.008	1.5	3.08	0.009	1.8	3.44	0.009	-1.85	109.00	0.0054
incl. Fe-O-O path[h]		(0.5)	(0.008)	(0.001)	(0.3)	(0.02)		(0.3)	(0.02)		(1.17)		

[a]The amplitude reduction factor S_0^2 was set to 0.9 based on first shell optimization for all sorption samples (R 1.1–2.5 Å). [b]Path degeneracy (coordination number). [c]Mean half path length. [d]Debye−Waller parameter. Debye−Waller parameter was fixed to 0.009 Å^2 for Fe-Fe of low Fe-loading sorption sample like was fitted for edge-sharing Fe-Fe for low Fe-loading samples. [e]Energy-shift parameter [f]Fit accuracy; reduced $\chi^2 = (N_{idp}/N_{pts})\sum_i ((data_i - fit_i)/\varepsilon_i)^2 (N_{idp}-N_{var})^{-1}$. N_{idp}, N_{pts} and N_{var} are, respectively, the number of independent points in the model fit (11.2), the total number of data points (171), and the number of fit variables (8). ε_i is the uncertainty of the i^{th} data point. [g]R-factor; Normalized sum of squared residuals ($\sum_i (data_i - fit_i)^2 / \sum_i data^2$). [h]Model is compared with model including a triangular Fe–O–O multiple scattering path constrained as follows: $N = 4CN_{Fe\text{–}O}$, $R = R_{Fe\text{–}O}(1 + \sqrt{2}/2)$, and $\sigma^2 = 2\sigma^2_{Fe\text{–}O}$.[18] Notes: Parameter uncertainties are given in parentheses.

16. Polarized EXAFS

Polarized-EXAFS (P-EXAFS) can be used to differentiate between the three shell fitting models (model 1, 2 and 3, see section 10) for the anoxic high Fe-loading samples. In P-EXAFS neighbouring atoms along the electric field (or along polarization direction of the X-ray beam) are preferentially probed, and atoms located in a plane perpendicular to this electric field direction are attenuated. Applying this method to clay mineral self-supporting films has the advantage of minimizing the contribution of cations from the tetrahedral sheets by orienting the layer ab plane to electric field and conversely, the contributions of cations from the octahedral sheet is extinguished in the perpendicular orientation of the electric field.

P-EXAFS of the self-supporting film of anoxic high Fe-loading sorption sample equilibrated at pH 8 are given in Figure S15. The $k^3\chi(k)$ spectra contained isosbestic points for which $\chi(k)$ is independent of k over the whole k range and the spectra displayed a large dependence of the $k^3\chi(k)$ spectra upon orientation in the regions between the isosbestic points. The presence of isosbestic provides a good evidence that differences in the measured spectra are due to orientation effects alone. The observed spectral dichroism confirms the oriented clay film were successfully prepared.[19-21] With P-EXAFS the effective number of atoms, called the apparent coordination number ($CN_{j,\alpha}^{exafs}$), seen at the angle (α) is detected.[19-22] The relationship between $CN_{j,\alpha}^{exafs}$ and the coordination number CN_j is given by the following equation:

$$CN_{j,\alpha}^{exafs}/CN_j = 1 - ((3\cos^2\beta_j - 1).(3\cos^2\alpha - 2))/2 \qquad (2)$$

With α being the angle between the film normal and the vector connecting the X-ray absorbing atom i to the backscattering atom j, CN_j is the crystallographic number of atoms in the j shell. When oriented films are at angle α = 35.3° ("magic angle") relative to the incoming beam, texture effects emerging from the anisotropy of the clay film are cancelled. Leading to a simplification of Eq. (2) to $CN_j = CN_{j,\alpha}^{exafs}$.[20, 21] Hence the radial distance (R) and Debye–Waller parameter (σ) for shell-by-shell fitting of the FT of the $k^3\chi(k)$ spectra of oriented sample at angle 10°, 55° and 80° were fixed to values obtained from the fit of FT of $k^3\chi(k)$ spectra at angle 35°.

The FT of the $k^3\chi(k)$ spectra of the oriented anoxic high Fe-loading samples displayed peaks at distances (uncorrected for phase shift) of ~1.5 Å and at ~2.8 Å (see Figure S14). The shell-by-shell fitting of FT of the $k^3\chi(k)$ spectra of both oriented samples were performed with model 1, 2 and 3 presented in section 10. First shell fitted with a Fe-O path and second shell with Fe-Fe path (model 1), Fe-Fe and Fe-Al (model 2) or Fe-Fe and Fe-Si paths (model 3). Both model 2 and 3 gave unsatisfactory fits for the FT of the $k^3\chi(k)$ spectra of oriented samples at angle 80°. Conversely model 1 which uses an Fe-Fe path for the 2nd shell lead to a good fit (R-factor < 2%) suggesting that in the direction perpendicular direction of the clay layers Fe is present and not Si or Al. Similarly, the FT of the $k^3\chi(k)$ EXAFS spectra at 10° angle lead to a unsatisfactory fit including Fe-Si or Fe-Al. Therefore, the model 2 and 3 could be excluded as models for the description of the coordination environment of Fe in anoxic high Fe-loading sorption samples. The amplitude of both shells decreases with increasing α (Figure S16) which is also reflected in Table S19 with CN(O) and CN(Fe) decreasing with increasing angle. This angular variation strengthens the assumption of an LDH like phase with Fe in the octahedral sheet for anoxic high Fe-loading samples.

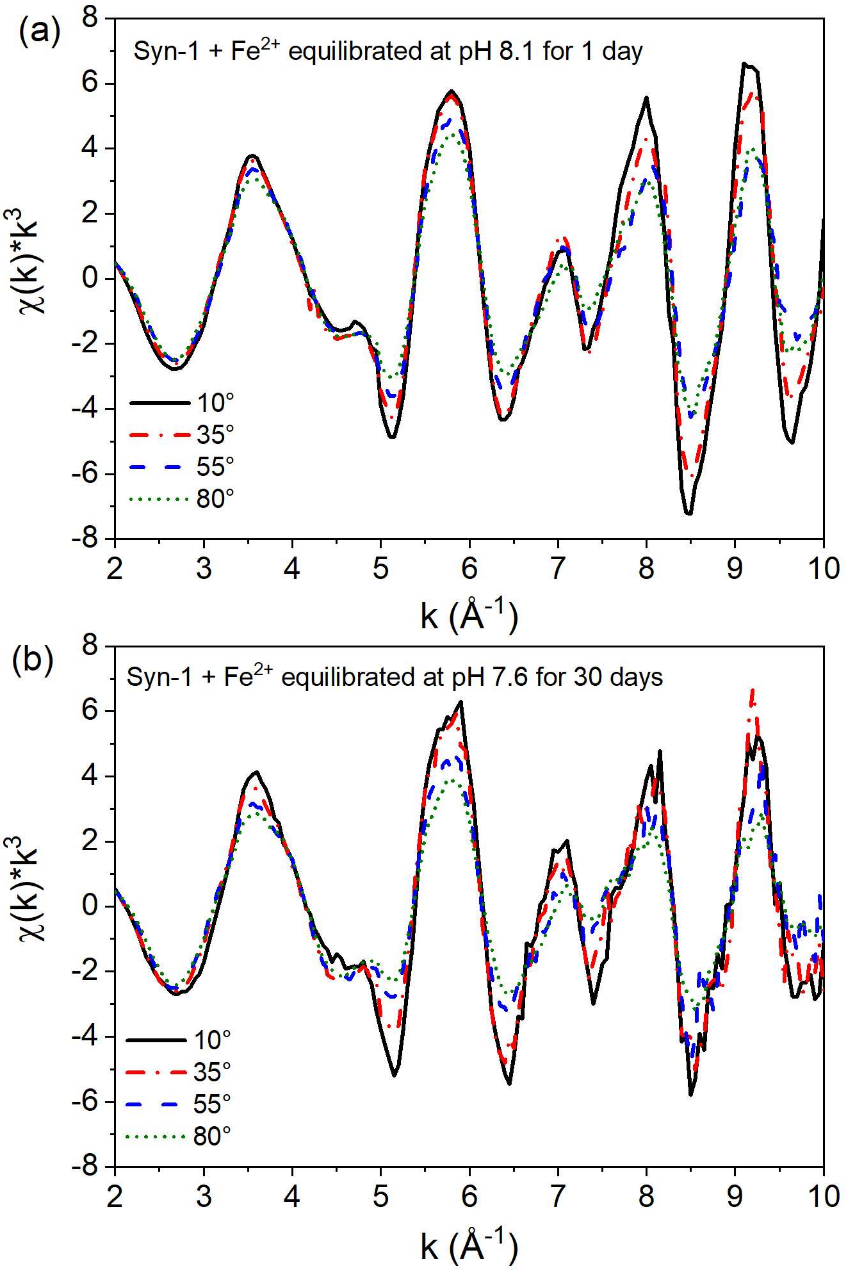

Figure S15: k^3-weighted Fe K-edge EXAFS spectra of a Fe-sorbed Syn-1 film at angles of 10°, 35°, 55° and 80°. Ferrous iron sorbed on Syn-1 at pH ~8 (0.5 mol Fe/kg clay) and equilibrated for 1 day (a) and 30 days (b).

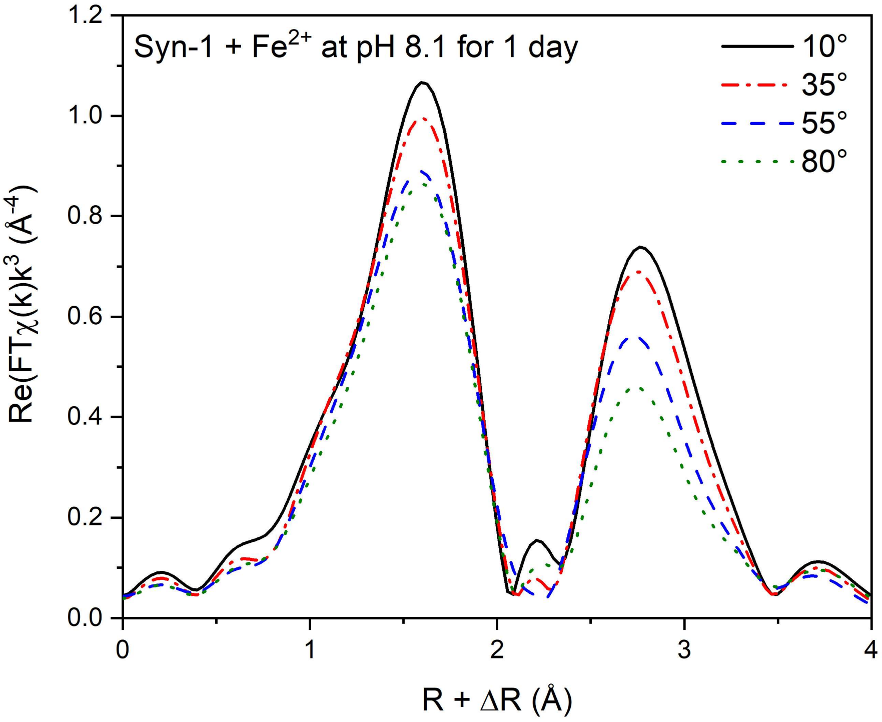

Figure S16: Polarization dependence of the Fourier transform from the Fe K-edge EXAFS spectra presented in Figure S13a.

Table S19: Shell-fit parameters determined for FT of Fe K-edge EXAFS spectra of oriented samples at angles 10°, 35°, 55°, 80° for anoxic high Fe-loading sample equilibrated for 1 day at pH 8.1. Use of Fe-Fe path for second RSF peak.[a]

		Fe-O				Fe-Fe						
angle	**CN**[b]	**±**	**R[Å]**[c]	**σ²[Å²]**[d]	**CN**	**±**	**R[Å]**	**σ²[Å²]**	ΔE_0^e	**±**	**Red. χ²** [f]	**R-factor**[g]
10°	4.8	0.5	2.12[h]	0.007[h]	3.2	0.4	3.21[h]	0.004[h]	0.4	0.8	238	0.0401
35°	4.3	0.7	2.12	0.007	3.0	0.2	3.21	0.004	0.2	1.4	212	0.0364
55°	3.9	0.3	2.12[h]	0.007[h]	2.4	0.2	3.21[h]	0.004[h]	0.9	0.6	373	0.0210
80°	3.8	0.3	2.12[h]	0.007[h]	1.9	0.2	3.21[h]	0.004[h]	0.9	0.6	216	0.0243

[a] The amplitude reduction factor S_0^2 was set to 0.9 based on first shell optimization for all sorption samples (R 1.1–2.5 Å). [b] Path degeneracy (coordination number). [c] Mean half path length. [d] Debye−Waller parameter. [e] Energy-shift parameter. [f] Fit accuracy; reduced $\chi^2 = (N_{idp}/N_{pts})\sum_i ((data_i - fit_i)/\varepsilon_i)^2 (N_{idp}-N_{var})^{-1}$. N_{idp}, N_{pts} and N_{var} are, respectively, the number of independent points in the model fit (10.3), the total number of data points (171), and the number of fit variables (3–7). ε_i is the uncertainty of the *i*th data point. [g] R-factor; Normalized sum of squared residuals ($\sum_i (data_i - fit_i)^2 / \sum_i data^2$). [h] Note: $R_{Fe\text{-}O}$, $R_{Fe\text{-}Fe}$, $\sigma^2_{Fe\text{-}O}$ and $\sigma^2_{Fe\text{-}Fe}$ were fixed to the value determined at α = 35°.[20]

Table S20: Shell-fit parameters determined for FT of Fe K-edge EXAFS spectra of oriented samples at angles 10°, 35°, 55°, 80° for anoxic high Fe-loading sample equilibrated for 30 days at pH 7.6. Use of Fe-Fe path for second RSF peak.[a]

	Fe-O				Fe-Fe							
angle	**CN**[b]	**±**	**R[Å]**[c]	**σ^2[Å^2]**[d]	**CN**	**±**	**R[Å]**	**σ^2[Å^2]**	ΔE_0^e	**±**	**Red. χ^2** [f]	**R-factor**[g]
10°	5.3	0.3	2.12[h]	0.009[h]	5.0	0.2	3.20[h]	0.008[h]	-3.4	0.3	9	0.0089
35°	5.4	1.0	2.12	0.009	4.3	0.4	3.20	0.004	-4.0	1.6	35	0.0119
55°	4.6	0.3	2.12[h]	0.009[h]	2.8	0.3	3.20[h]	0.008[h]	-3.8	0.5	22	0.0178
80°	4.1	0.2	2.12[h]	0.009[h]	2.2	0.2	3.20[h]	0.008[h]	-3.3	0.6	77	0.0185

[a] The amplitude reduction factor S_0^2 was set to 0.9 based on first shell optimization for all sorption samples (R 1.1–2.5 Å). [b] Path degeneracy (coordination number). [c] Mean half path length. [d] Debye–Waller parameter. [e] Energy-shift parameter. [f] Fit accuracy; reduced $\chi^2 = (N_{idp}/N_{pts})\sum_i ((data_i - fit_i)/\varepsilon_i)^2 (N_{idp}-N_{var})^{-1}$. N_{idp}, N_{pts} and N_{var} are, respectively, the number of independent points in the model fit (10.3), the total number of data points (171), and the number of fit variables (3–7). ε_i is the uncertainty of the *i*th data point. [g] R-factor; Normalized sum of squared residuals ($\sum_i (data_i - fit_i)^2 / \sum_i data^2$). [h] Note: R_{Fe-O}, R_{Fe-Fe}, σ^2_{Fe-O} and σ^2_{Fe-Fe} were fixed to the value determined at α = 35°.[20]

References

1. B. Ravel and M. Newville, ATHENA, ARTEMIS, HEPHAESTUS: data analysis for X-ray absorption spectroscopy using IFEFFIT, *J. Synchrotron Radiat.*, 2005, **12**, 537-541.
2. S. M. Webb, SIXpack: a graphical user interface for XAS analysis using IFEFFIT, *Phys. Scr.*, 2005, **T115**, 1011-1014.
3. E. R. Malinowski, Theory of error for target factor-analysis with applications to mass-spectrometry and nuclear magnetic-resonance spectrometry, *Anal. Chim. Acta*, 1978, **2**, 339-354.
4. J. Mustre de Leon, J. J. Rehr, S. I. Zabinsky and R. C. Albers, Ab initio curved-wave x-ray-absorption fine structure, *Phys. Rev. B*, 1991, **44**, 4146-4156.
5. J. J. Rehr, S. I. Zabinsky, A. Ankudinov and R. C. Albers, Atomic-XAFS and XANES, *Physica B*, 1995, **208**, 23-26.
6. F. Trolard, G. Bourrie, M. Abdelmoula, P. Refait and F. Feder, Fougerite, a new mineral of the pyroaurite-iowaite group: Description and crystal structure, *Clay Clay Miner*, 2007, **55**, 323-334.
7. N. Kaur, B. Singh, B. J. Kennedy and M. Grafe, The preparation and characterization of vanadium-substituted goethite: The importance of temperature, *Geochim. Cosmochim. Acta*, 2009, **73**, 582-593.
8. H. Shirozu and S. W. Bailey, Chlorite Polytypism .3. crystal structure of an orthohexagonal iron chlorite, *Am. Mineral.*, 1965, **50**, 868-&.
9. D. M. C. Huminicki and F. C. Hawthorne, The crystal structure of nikischerite, Na $Fe^{2+}{}_6$ $Al_3(SO_4)_2 (OH)_{18} (H_2O)_{12}$, a mineral of the shigaite group, *Can. Mineral.*, 2003, **41**, 79-82.

10. A. P. Zhukhlistov, Crystal structure of lepidocrocite FeO(OH) from the electron-diffractometry data, *Crystallogr. Rep.*, 2001, **46**, 730-733.
11. D. Soltermann, M. Marques Fernandes, B. Baeyens, R. Dähn, J. Miehé-Brendlé, B. Wehrli and M. H. Bradbury, Fe(II) sorption on a synthetic montmorillonite. A combined macroscopic and spectroscopic study, *Environ. Sci. Technol.*, 2013, **47**, 6978-6986.
12. M. G. Newville and B. Ravel, Developments of advanced XAFS analysis techniques with Ifeffit, *Acta Crystallogr. A.*, 2008, **64**, C66-C66.
13. M. Newville, IFEFFIT: interactive XAFS analysis and FEFF fitting, *J. Synchrotron Radiat.*, 2001, **8**, 322-324.
14. E. A. Stern, Number of relevant independent points in X-ray-absorption fine-structure spectra, *Phys. Rev. B*, 1993, **48**, 9825-9827.
15. L. Downward, C. H. Booth, W. W. Lukens and F. Bridges, *A variation of the F-Test for determining statistical relevance of particular parameters in EXAFS fits*, Report 0094-243x, 2007.
16. H. Funke, A. C. Scheinost and M. Chukalina, Wavelet analysis of extended x-ray absorption fine structure data, *Phys. Rev. B*, 2005, **71**.
17. S. D. Kelly, B. Hesterdberg and B. Ravel, in *Methods of Soil Analysis Part 5—Mineralogical Methods, SSSA Book Ser. 5.5. SSSA*, ed. L. R. D. A. L. ULERY, Madison, WI, 2008, DOI: DOI 10.2136/sssabookser5.5.c14, pp. 387-463.
18. C. Mikutta, X-ray absorption spectroscopy study on the effect of hydroxybenzoic acids on the formation and structure of ferrihydrite, *Geochim. Cosmochim. Acta*, 2011, **75**, 5122-5139.
19. A. Manceau and M. L. Schlegel, Texture effect on polarized EXAFS amplitude, *Phys. Chem. Miner.*, 2001, **28**, 52-56.
20. A. Manceau, D. Chateigner and W. P. Gates, Polarized EXAFS, distance-valence least-squares modeling (DVLS), and quantitative texture analysis approaches to the structural refinement of Garfield nontronite, *Phys. Chem. Miner.*, 1998, **25**, 347-365.
21. A. Manceau, D. Bonnin, P. Kaiser and C. Fretigny, Polarized EXAFS of Biotite and Chlorite, *Phys. Chem. Miner.*, 1988, **16**, 180-185.
22. Schlegel M. L., Manceau A., Charlet L. and Hazemann J. L., Adsorption mechanisms of Zn on hectorite as a function of time, pH, and ionic strength, *Am. J. Sci.*, 2001, **301**, 798-830.